Available online at www.sciencedirect.com
SCIENCE DIRECT®
Journal of Sound and Vibration 292 (2006) 969–979
JOURNAL OF SOUND AND VIBRATION
www.elsevier.com/locate/jsvi

Short Communication

Perturbation analysis of a clearance-type nonlinear system

Farong Zhu, Robert G. Parker*

Department of Mechanical Engineering, The Ohio State University, Columbus, OH 43202, USA

Received 23 June 2005; received in revised form 23 June 2005; accepted 24 August 2005
Available online 17 November 2005

Abstract

This study applies the method of multiple scales to obtain periodic solutions of a two-pulley belt system with clearance-type nonlinearity. The purpose is to explain the published numerical results and clarify how design parameters affect the system dynamics. The validity of the perturbation method for such strong nonlinearity is evaluated. The closed-form frequency–response relation is determined at the first order, and an implicit expression is obtained for the second-order approximation. The preload applied to the accessory determines the softening level of the nonlinearity. Larger preload leads to less disengagement and less softening. For a considerable range of practical parameter values, the analytical solutions well approximate the numerical results from harmonic balance.

1. Introduction

A two-pulley system with clearance-type nonlinearity is illustrated in Fig. 1(a). An application of this system has been presented in Ref. [1], where a discontinuous separation function models the alternate engagement and disengagement of the pulley and accessory that functions through a one-way clutch. In Ref. [1], the harmonic balance method with arc-length continuation is employed. Results show a rich picture of stable and unstable periodic solutions when the system operates across a range of excitation frequencies. The present work pursues analytical periodic solutions of this system in order to explain the numerical results and clarify how the design parameters affect the dynamics.

Perturbation analysis to obtain periodic solutions of dynamic systems is most commonly applied to weak nonlinearities. A few studies (e.g., Refs. [2–5]) deal with the validity of this technique for strongly nonlinear systems, where the Lindstedt–Poincaré perturbation scheme is extended. For discontinuous nonlinearities with piecewise linear or weakly nonlinear characteristics, piecewise analytical methods are generally employed [6–8] where the perturbation technique is used for each linear or nonlinear piece.

The current study applies the method of multiple scales to the system with clearance-type nonlinearity shown in Fig. 1(a) and evaluates the validity of the method for such strong nonlinearity. The discontinuous function is expanded as a Fourier series, where the Fourier coefficients are evaluated for given excitation amplitude. The closed-form frequency–response relation is determined at the first order. Periodic

*Corresponding author. Tel.: +1 614 688 3922; fax: +1 614 292 3163.
E-mail address: parker.242@osu.edu (R.G. Parker).

0022-460X/$ - see front matter © 2005 Elsevier Ltd. All rights reserved.
doi:10.1016/j.jsv.2005.08.025

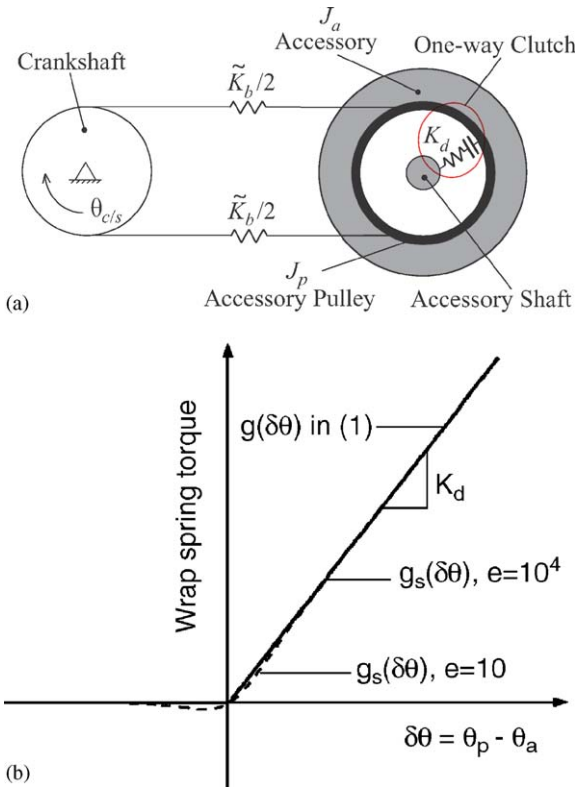

Fig. 1. (a) A two-pulley belt system; (b) wrap-spring torque $g(\delta\theta)$ in Eq. (1) and the smoothed function $g_s(\delta\theta)$ according to Eq. (3) for different smoothing parameters e.

approximations are determined up to the second order. The system is analyzed for a range of excitation frequency with different preload values to characterize, where the power transmission is most efficient.

2. System model

The driving pulley in Fig. 1(a) is subject to periodic motion excitation specified as $\theta_{c/s} = A_m \cos \Omega T$, and the power is transmitted to the driven pulley through a belt modeled as springs with stiffness $\tilde{K}_b/2$. The driven pulley and the accessory shaft are connected with a wrap spring of stiffness K_d that is disconnected when the pulley and the shaft are disengaged. An accessory that acts as a load is rigidly connected to the shaft. The system shows clearance-type nonlinearity when the pulley and shaft are alternately engaged and disengaged. When the rotations of the wrap-spring ends are such that the pulley rotation θ_p exceeds the accessory shaft rotation θ_a, the clutch is engaged. Alternately, when pulley rotation is less than accessory rotation, the wrap-spring diameter decreases and the clutch disengages. Only engagement of the pulley and shaft allows power transmission to the accessory. The wrap-spring torque is mathematically expressed in the dimensionless form (Fig. 1(b))

$$g(\delta\theta) = \begin{cases} K_d \delta\theta, & \delta\theta > 0, \\ 0, & \delta\theta \leqslant 0, \end{cases} \tag{1}$$

where $\delta\theta = \theta_p - \theta_a$. The equations of motion for the pulley and accessory are

$$\begin{bmatrix} J_p & 0 \\ 0 & J_a \end{bmatrix} \ddot{\boldsymbol{\theta}} + \mathbf{C}\dot{\boldsymbol{\theta}} + \begin{bmatrix} K_b & 0 \\ 0 & 0 \end{bmatrix} \boldsymbol{\theta} + \begin{pmatrix} g(\delta\theta) \\ -g(\delta\theta) \end{pmatrix} = \begin{pmatrix} M + K_b \beta A_m \cos \Omega t \\ -M \end{pmatrix}, \tag{2}$$

Table 1
Nomenclature and dimensionless parameter values for nominal case

$r_p = 1$	Radius of pulley
$r_c = 1.422$	Radius of driving pulley
$J_p = 1$	Pulley inertia
$J_a = 1.620$	Accessory inertia
$\zeta_1, \zeta_2 = 3\%$	Modal damping ratios
$K_b = 2.620$	Belt stiffness
$K_d = 27.66$	Wrap spring stiffness
$A_m = 0.001$	Excitation amplitude
$M = 0.0127$	Preload

where $\boldsymbol{\theta} = \{\theta_p \ \ \theta_a\}^{\mathrm{T}}$, $K_b = \tilde{K}_b r_p^2$, $\beta = r_c/r_p$, and the dot denotes the time derivative $\mathrm{d}/\mathrm{d}t$. $\mathbf{C}$ is computed from the modal damping matrix of the two-dof linear system with the pulley and shaft engaged. See Table 1 for the nomenclature and dimensionless parameter values.

A hyperbolic tangent function

$$g_s(\delta\theta) = K_d \delta\theta f_g, \quad f_g = \tfrac{1}{2}[1 + \tanh(e\delta\theta)] \tag{3}$$

is employed in Ref. [1] to approximate $g(\delta\theta)$ for multiple methods. According to Ref. [1], use of $e = 10,000$ in Eq. (3) ensures accuracy (Fig. 1(b)). In the following, the original discontinuous function (1) is considered and the results are compared with those from harmonic balance using Eq. (3).

3. Perturbation analysis

The method of multiple scales is frequently used to obtain periodic approximations for systems with continuous, weak nonlinearity [9]. This yields closed-form approximations for the frequency–response curve. Furthermore, it can provide theoretical explanation for phenomena observed by numerical methods. Here, the method of multiple scales is employed for the system in Eq. (2) but rewritten as

$$\begin{bmatrix} J_p & 0 \\ 0 & J_a \end{bmatrix} \ddot{\boldsymbol{\theta}} + \mathbf{C}\dot{\boldsymbol{\theta}} + \begin{bmatrix} K_b + K_d & -K_d \\ -K_d & K_d \end{bmatrix} \boldsymbol{\theta} + \begin{pmatrix} h(\delta\theta) \\ -h(\delta\theta) \end{pmatrix} = \begin{pmatrix} M + K_b \beta A_m \cos \Omega t \\ -M \end{pmatrix}, \tag{4}$$

$$h = -K_d \delta\theta f(\delta\theta), \quad f(\delta\theta) = \begin{cases} 0, & \delta\theta \geqslant 0, \\ 1, & \delta\theta < 0. \end{cases} \tag{5}$$

Let $\mathbf{U}$ be the orthonormalized modal matrix of the linear undamped system. Letting $\boldsymbol{\theta} = \mathbf{U}\mathbf{q}$, one obtains the decoupled form with modal coordinates $\mathbf{q}$ as

$$\ddot{q}_i + 2\varsigma_i \Omega_i \dot{q}_i + \Omega_i^2 q_i + H_i(\delta\theta) = M_i + \tilde{B}_i \cos \Omega t, \quad i = 1, 2, \tag{6}$$

where Ω_i are the linear undamped natural frequencies of Eq. (4), $H_i(\delta\theta) = \gamma_i h(\delta\theta)$ with $\gamma_i = u_{1i} - u_{2i}$ and $\delta\theta = \gamma_1 q_1 + \gamma_2 q_2$, $M_i = \gamma_i M$ and $\tilde{B}_i = u_{1i} K_b \beta A_m$.

The separation function $f(\delta\theta)$ in Eq. (5) is expanded as a Fourier series. To be consistent with numerical results in Ref. [1], where the response is periodic at the excitation frequency, Ω is the fundamental frequency of $f(\delta\theta)$, that is,

$$f = \hat{f}_0 + \left(\sum_{k=1}^{\infty} \hat{f}_k \mathrm{e}^{\mathrm{j}k\Omega t} + \text{c.c.} \right), \tag{7}$$

where c.c. denotes complex conjugate. To introduce a perturbation parameter, let ε be the fraction of the response period, T, where the pulley and shaft are disengaged. This assumption and another that only a single disengagement occurs per cycle lead to Fourier coefficients $\hat{f}_k$, $k \geqslant 0$, that are all order ε (demonstrated later).

Therefore, one can write Eq. (7) as

$$f = \varepsilon\left[\tilde{f}_0 + \left(\sum_{k=1}^{\infty} \tilde{f}_k e^{jk\Omega t} + \text{c.c.}\right)\right] = \varepsilon\tilde{f},$$

where $\tilde{f}_k = \hat{f}_k/\varepsilon = O(1)$.

The quantities $t_0 = t$ and $t_n = \varepsilon^n t,\ n \geqslant 1$ are fast and slow times, respectively. The differential operators and the response are expanded as

$$\frac{d}{dt} = D_0 + \varepsilon D_1 + \varepsilon^2 D_2 + O(\varepsilon^3), \quad \frac{d^2}{dt^2} = D_0^2 + 2\varepsilon D_0 D_1 + \varepsilon^2(D_1^2 + 2D_0 D_2) + O(\varepsilon^3), \tag{8}$$

$$q_i = q_{i0}(t_0, t_1, t_2) + \varepsilon q_{i1}(t_0, t_1, t_2) + \varepsilon^2 q_{i2}(t_0, t_1, t_2) + O(\varepsilon^3). \tag{9}$$

Considering the second primary resonance as an example, the excitation frequency is $\Omega = \Omega_2 + \varepsilon\sigma$, where σ is a detuning parameter. Internal resonance is not considered. The dynamic excitation and damping are specified as $O(\varepsilon)$ according to $\tilde{B}_i = \varepsilon B_i$ and $\varsigma_i\omega_i = \varepsilon\mu_i$. Substitution of Eq. (8) and (9) into Eq. (6) gives

$$D_0^2 q_{i0} + \Omega_i^2 q_{i0} = M_i, \tag{10}$$

$$D_0^2 q_{i1} + \Omega_i^2 q_{i1} = -2\mu_i D_0 q_{i0} - 2D_0 D_1 q_{i0} - H_{i1} + B_i \cos\Omega t_0, \tag{11}$$

$$D_0^2 q_{i2} + \omega_i^2 q_{i2} = -2\mu_i D_1 q_{i0} - 2\mu_i D_0 q_{i1} - 2D_0 D_1 q_{i1} - D_1^2 q_{i0} - 2D_0 D_2 q_{i0} - H_{i2}, \tag{12}$$

for $i = 1, 2$, and where H_{i1} and H_{i2} include the ε^1, ε^2 order terms in H_i, respectively.

3.1. First-order approximation

The leading order approximation from Eq. (10) is

$$q_{i0}(t_0, t_1, t_2) = m_i + [A_i(t_1, t_2)e^{j\Omega_i t_0} + \text{c.c.}], \tag{13}$$

where $A_i(t_1, t_2)$ is the unknown amplitude and $m_i = M_i/\Omega_i^2$. The solvability conditions generated from Eq. (11) are

$$2j\Omega_1 D_1 A_1 = (-2\mu_1 j\Omega_1 + \gamma_1^2 K_d \tilde{f}_0)A_1,$$

$$2j\Omega_2 D_1 A_2 = -2\mu_2 j\Omega_2 A_2 + \gamma_2 K_d[\gamma_2 A_2 \tilde{f}_0 + (\gamma_1 m_1 + \gamma_2 m_2)\tilde{f}_1 e^{j\sigma t_1} + \gamma_2 \bar{A}_2 \tilde{f}_2 e^{j2\sigma t_1}] + b_2 e^{j\sigma t_1}, \tag{14}$$

with $b_i = B_i/2$. The overbar denotes complex conjugate. At the steady state, $A_1 \to 0$ as $t_1 \to \infty$ from the first equation (14). This trivial solution guarantees the response has the fundamental frequency $\Omega \approx \Omega_2$ according to $\delta\theta = \gamma_1 q_{10} + \gamma_2 q_{20} + O(\varepsilon)$. Now one can take

$$A_i(t_1, t_2) = a_i(t_1, t_2)e^{j\beta_i(t_1, t_2)}/2, \quad i = 1, 2 \tag{15}$$

and write q_{20} as the real form $q_{20} = a_2 \cos(\Omega_2 t_0 + \beta_2) + m_2$. Because

$$\delta\theta \approx \gamma_2[a_2 \cos(\Omega_2 t_0 + \beta_2) + m_2] + \gamma_1 m_1, \tag{16}$$

the Fourier coefficients of $f(\delta\theta)$ are

$$\hat{f}_0 = \frac{\Omega}{2\pi}\int_0^{2\pi/\Omega} f(\delta\theta)\, dt_0 \overset{\phi=\Omega_2 t_0+\beta_2}{=} \frac{1}{2\pi}\int_0^{2\pi} f(\delta\theta)\, d\phi,$$

$$\hat{f}_k = \frac{1}{2\pi} e^{jk(\beta_2 - \sigma t_1)} \int_0^{2\pi} f(\delta\theta) e^{-jk\phi}\, d\phi. \tag{17}$$

In Eq. (17), t_1 varies slowly compared to t_0 and is considered as a constant in the integrals. To evaluate the integrals in Eq. (17), identification of the region where $\delta\theta < 0$ (giving $f(\delta\theta) = 1$ from Eq. (5)) is needed (see

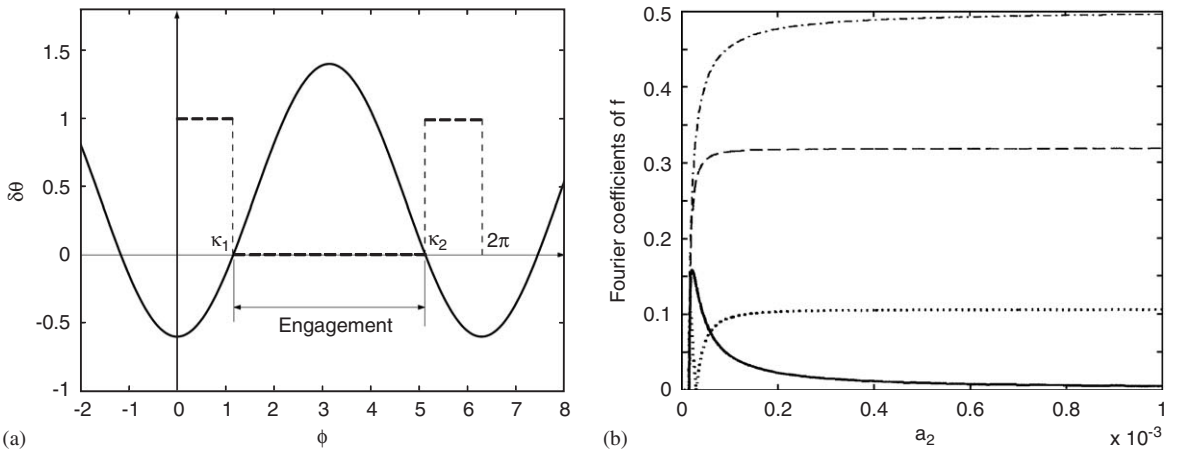

Fig. 2. (a) The integration intervals for Eqs. (17)–(19) and separation function $f(\delta\theta)$ (- -) as $\gamma_2<0$. (b) Magnitudes of Fourier coefficients of the separation function f vary with the response amplitude a_2 for $M=0.0127$. $|f_0|$ (- -), $|\chi_1|$ (- -), $|\chi_2|$ (—), $|\chi_3|$ (·····).

Fig. 2(a)). The critical phases $\phi=\kappa_1,\kappa_2$ are obtained from $\delta\theta=0$ as

$$\cos\phi|_{\phi=\kappa_1,\kappa_2}=-\frac{(\gamma_1 m_1+\gamma_2 m_2)}{\gamma_2 a_2}=-\frac{(\gamma_1^2/\Omega_1^2+\gamma_2^2/\Omega_2^2)M}{\gamma_2 a_2}=x. \tag{18}$$

Here the case of $\gamma_2<0$ is discussed ($\gamma_2>0$ generates the same results). The integration interval is $[0,\kappa_1]\cup[\kappa_2,2\pi]$, where $\kappa_1=\cos^{-1}x$ and $\kappa_2=2\pi-\cos^{-1}x$. For $x>1$ there is no separation and the pulley and shaft are always engaged. In this case, $f(\delta\theta)=0$ and the system operates linearly. On the other hand, $x<-1$ implies the pulley and shaft are disengaged for the entire cycle and $f(\delta\theta)=1$. Further expansion of Eq. (17) gives

$$\hat{f}_0=\kappa_1/\pi,\quad \hat{f}_k=\chi_k e^{ik(\beta_2-\sigma t_1)},\quad \chi_k=\sin k\kappa_1/k\pi\quad \text{for } k\geqslant 1. \tag{19}$$

For a given belt stiffness K_b and wrap spring stiffness K_d, the preload M affects the separation for a given amplitude a_2. A positive preload acts against separation and promotes power transmission, while negative preload promotes separation. For the parameters in Table 1, $\gamma_2<0$ and, according to Eq. (18), $x\geqslant 0$ for $M\geqslant 0$. Therefore, for any vibration amplitude where disengagement occurs, $0<\kappa_1\leqslant\pi/2$. This is consistent with the prior assumption that κ_1/π is small. Also, $\hat{f}_0\in[0,0.5]$. The mean value $|\hat{f}_0|$ of the separation function f is greater than any harmonic amplitude $|\chi_k|$ because $|\chi_k|=|\sin k\kappa_1/k\pi|\leqslant|\kappa_1/\pi|=|\hat{f}_0|$ (Fig. 2(b)). All these validate the earlier stipulation that $\hat{f}_0,\hat{f}_k=O(\varepsilon)$. In the following, let $\tilde{\chi}_k=\chi_k/\varepsilon$.

Separation of the real and imaginary parts of Eq. (14) yields

$$\Omega_1 D_1 a_1=-\Omega_1\mu_1 a_1,\quad -\Omega_1 a_1 D_1\beta_1=\tfrac{1}{2}\gamma_1^2 K_d\tilde{f}_0 a_1, \tag{20}$$

$$\Omega_2 D_1 a_2=-\Omega_2\mu_2 a_2+b_2\sin\lambda,$$

$$\Omega_2 a_2 D_1\lambda=\Omega_2 a_2\sigma+\gamma_2 K_d[\tfrac{1}{2}\gamma_2 a_2\tilde{f}_0+(\gamma_1 m_1+\gamma_2 m_2)\tilde{\chi}_1+\tfrac{1}{2}\gamma_2 a_2\tilde{\chi}_2]+b_2\cos\lambda, \tag{21}$$

where $\lambda=\sigma t_1-\beta_2$. Considering the steady-state motion where $D_1(\cdot)=0$, the frequency–response relation from Eqs. (20) and (21) is $a_1=0$ and

$$\sigma=-R\pm\sqrt{\frac{b_2^2}{\Omega_2^2 a_2^2}-\mu_2^2},\quad R=\frac{\gamma_2 K_d}{\Omega_2}\left[\frac{1}{2}\gamma_2\tilde{f}_0+(\gamma_1 m_1+\gamma_2 m_2)\frac{\tilde{\chi}_1}{a_2}+\frac{1}{2}\gamma_2\tilde{\chi}_2\right]. \tag{22}$$

3.2. Second-order approximation

To seek second-order approximations, the reconstitution procedure [10–13] is adopted. After eliminating secular terms, the particular solutions $q_{i1}(t)$ of Eq. (11) are obtained. Substitution of $q_{i1}(t)$ into Eq. (12) and collection of the secular terms of Eq. (12) lead to the solvability conditions

$$-2\mathrm{j}\Omega_1 D_2 A_1 - D_1^2 A_1 - 2\mu_1 D_1 A_1 + I_1 A_1 = 0, \tag{23}$$

$$-2\mathrm{j}\Omega_2 D_2 A_2 - D_1^2 A_2 - 2\mu_2 D_1 A_2 + I_1 = 0, \tag{24}$$

where $I_1 = I_1(\tilde{f}_0, \tilde{\chi}_k)$ and $I_2 = I_2(\tilde{f}_0, \tilde{\chi}_k, A_2, \sigma)$ are collected from H_{i2} in Eq. (12). $D_1^2 A_i$ in Eqs. (23) and (24) are determined by differentiating Eq. (14) with respect to t_1. Substitution of Eq. (15) into Eqs. (23) and (24) and separation of their real and imaginary parts yield

$$\Omega_1 D_2 a_1 = -\frac{K_d \gamma_1^2}{2\Omega_1}\mu_1 \eta_0 a_1^2, \quad -\Omega_1 a_1 D_2 \beta_1 = \frac{1}{2} a_1 \left(\mu_1^2 + \frac{K_d^2 \gamma_1^4 \tilde{f}_0^2}{\Omega_1^2} - I_1\right), \tag{25}$$

$$\Omega_2 D_2 a_2 = r_1 + r_{11}\sin\lambda + r_{12}\cos\lambda, \quad \Omega_2 a_2 D_2 \lambda = r_2 + r_{21}\sin\lambda + r_{22}\cos\lambda. \tag{26}$$

$\eta_k, k \geqslant 0$ are determined by differentiating the Fourier coefficients $\tilde{f}_0$, $\tilde{\chi}_k$ with respect to t_1 as $D_1\tilde{f}_0 = \eta_0 D_1 a_2$ and $D_1\tilde{\chi}_k = \eta_k D_1 a_2$ for $k \geqslant 1$, where

$$\eta_0 = \frac{x}{\varepsilon 2\pi a_2\sqrt{1-x^2}}, \quad \eta_k = \frac{x\cos(k\cos^{-1}x)}{\varepsilon\pi a_2\sqrt{1-x^2}}, \quad k = 1, 2, \ldots \tag{27}$$

for $|x| < 1$. When $|x| \geqslant 1$, $\eta_k = 0$. r_{1i} and r_{2i} consist of the coefficients of $\sin\lambda$ and $\cos\lambda$, respectively. r_i is the collection of all terms except those with $\sin\lambda$ and $\cos\lambda$ as coefficients. For steady-state motion,

$$\frac{\mathrm{d}a_i(t_1, t_2)}{\mathrm{d}t} = \varepsilon D_1 a_i + \varepsilon^2 D_2 a_i + O(\varepsilon^3) = 0,$$

$$\frac{\mathrm{d}\beta_i(t_1, t_2)}{\mathrm{d}t} = \varepsilon D_1 \beta_i + \varepsilon^2 D_2 \beta_i + O(\varepsilon^3) = 0. \tag{28}$$

Therefore, by combining Eq. (20) with Eq. (25), and Eq. (21) with Eq. (26), the steady-state equations are

$$-\varepsilon\mu_1 a_1 - \varepsilon^2 \frac{K_d\gamma_1^2\mu_1\eta_0 a_1^2}{2\Omega_1^2} + O(\varepsilon^3) = 0,$$

$$-\frac{1}{2\Omega_1}\left[\varepsilon K_d\gamma_1^2\tilde{f}_0 + \varepsilon^2\left(\mu_1^2 + \frac{K_d^2\gamma_1^4\tilde{f}_0^2}{\Omega_1^2} - I_1\right)\right] + O(\varepsilon^3) = 0, \tag{29}$$

$$\frac{1}{\Omega_2}[\varepsilon(-\Omega_2\mu_2 a_2 + b_2\sin\lambda) + \varepsilon^2(r_1 + r_{11}\sin\lambda + r_{12}\cos\lambda)] + O(\varepsilon^3) = 0,$$

$$\frac{\varepsilon}{\Omega_2 a_2}\{\Omega_2 a_2\sigma + \gamma_2 K_d[\gamma_2 a_2\tilde{f}_0 + 2(\gamma_1 m_1 + \gamma_2 m_2)\tilde{\chi}_1] + b_2\cos\lambda\} + \frac{\varepsilon^2}{\Omega_2 a_2}(r_2 + r_{21}\sin\lambda + r_{22}\cos\lambda) + O(\varepsilon^3) = 0. \tag{30}$$

Clearly, $a_1 = 0$ is a solution of Eq. (29), which implies the first mode is not excited at all. By ignoring $O(\varepsilon^3)$ terms, Eq. (30) is rewritten as

$$\frac{\varepsilon}{\Omega_2}(Y_1 + Y_{11}\sin\lambda + Y_{12}\cos\lambda) = 0, \quad \frac{\varepsilon}{\Omega_2 a_2}(Y_2 + Y_{21}\sin\lambda + Y_{22}\cos\lambda) = 0,$$

$$Y_1 = -\Omega_2\mu_2 a_2 + \varepsilon r_1, \quad Y_2 = \Omega_2 a_2\sigma + \gamma_2 K_d[\gamma_2 a_2\tilde{f}_0 + 2(\gamma_1 m_1 + \gamma_2 m_2)\tilde{\chi}_1] + \varepsilon r_2,$$

$$Y_{11} = b_2 + \varepsilon r_{11}, \quad Y_{12} = \varepsilon r_{12}, \quad Y_{21} = \varepsilon r_{21}, \quad Y_{22} = b_2 + \varepsilon r_{22}. \tag{31}$$

The elimination of $\sin\lambda$ and $\cos\lambda$ by using common algebraic manipulations and trigonometric identities yields a polynomial in σ. For chosen amplitude a_2, one finds the roots of the polynomial. Consequently, the frequency–response relation analogous to Eq. (22) but at a higher order is generated.

4. Results and discussions

The first-order approximation from Eq. (22) is shown in Fig. 3 for parameters given in Table 1. To implement the stability analysis of the steady-state motions at (a_{20}, λ_0) from Eq. (21), a small variation $\mathbf{v} = \{\alpha, \vartheta\}^{\mathrm{T}}$ near a steady state is introduced as

$$a_2 = a_{20} + \alpha, \quad \lambda = \lambda_0 + \vartheta. \tag{32}$$

Substitution of Eq. (32) into Eq. (21) yields $D_1\mathbf{v} = \mathbf{J}\mathbf{v} + O(\mathbf{v})$, where $\mathbf{J}$ is the Jacobian matrix consisting of the first-order derivatives with respect to (α, ϑ) evaluated at (a_{20}, λ_0). The real parts of the eigenvalues of $\mathbf{J}$ determine the stability at steady state (a_{20}, λ_0). One can prove that the arc between the turning points P_1 and P_2 is unstable (see Fig. 3) [9]. Other than this arc, the solutions are stable.

In comparison with the results yielded by numerical integration and multi-term harmonic balance with arc-length continuation, the perturbation approximation generates lower maximum amplitude with less softening nonlinearity. According to Eq. (22), the maximum amplitude is determined by

$$a_2 = |b_2/\Omega_2\mu_2|, \tag{33}$$

where $b_2 = u_{12}K_b\beta A_m/2\varepsilon$. This is identical to the maximum amplitude of the linear system. The terms outside the square root in Eq. (22), $-R$, give the backbone curve. The backbone is affected only by the mean value and the first two harmonics of the separation function. These two issues are limitations of the first-order solution.

The transition frequencies where the disengagement begins and ends can be determined through the backbone terms $-R$ in Eq. (22). For the linear case, $\tilde{f}_0$, $\tilde{\chi}_k$ in R are all zero. The transition frequencies occur when $\tilde{f}_0$, $\tilde{\chi}_k$ start to be non-zero, which corresponds to a maximum amplitude a_{cr} above which the system behaves nonlinearly (shown in Fig. 2(b)). For the nominal case, $\Omega_{\mathrm{cr}} \approx 6.24, 7.38$, where points P_1 and P_7 are located correspondingly in Fig. 3. These values are consistent with the numerical results and those from analytical single-term harmonic balance.

The second-order approximation somewhat improves the amplitude and softening nonlinearity of the resonant peak in Fig. 3. Determination of the Fourier coefficients (17) and (19) is the same as for the first-order case, which limits the improvement from a second-order approximation. Corresponding to the points P_3 and P_5 in Fig. 3, where the maximum amplitude of the first-order approximation is $a_2 = 4.3 \times 10^{-5}$ (rms of $\delta\theta$

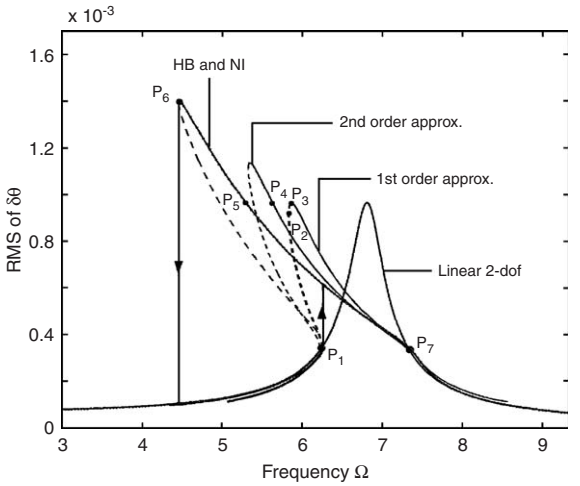

Fig. 3. The rms of $\delta\theta$ at the 2nd primary resonance yielded by the method of multiple scales, multi-term harmonic balance (HB) and numerical integration (NI) for the parameters in Table 1. Stable (——); unstable (- - -).

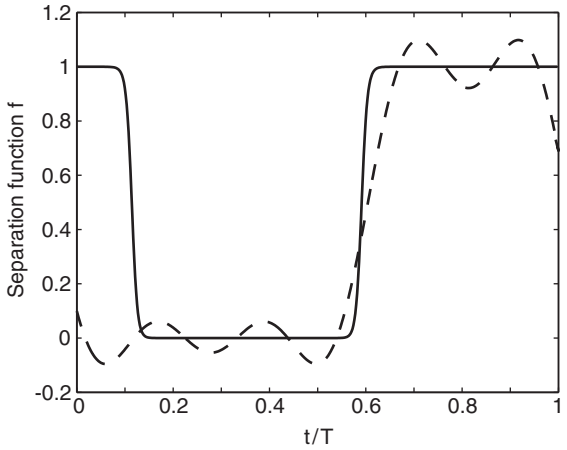

Fig. 4. Separation function f varies with time for points P_3 and P_5 in Fig. 3, where rms of $\delta\theta$ is 9.64×10^{-4} ($a_2 = 4.3 \times 10^{-5}$): ——, f_g in Eq. (3) at P_5, from multi-term harmonic balance; - - -, analytical solution at P_3, from four-term truncated Fourier series.

is 9.64×10^{-4}), the time histories of the separation function f in Eq. (5) are developed in Fig. 4. The smoothing function f_g in Eq. (3) is used for multi-term harmonic balance, while a four-term Fourier series of f is used for the analytical approximation. Note that the point P_4 with $a_2 = 4.3 \times 10^{-5}$ on the second-order branch in Fig. 3 has a similar shape of time history for f as P_3, although a phase difference exists. Apparently, the prediction of the separation (when $f \approx 1$) from the method of multiple scales is poorer than that from multi-term harmonic balance where half-period of the disengagement is shown. It is hard for the procedures (16)–(19) to determine half-time separation ($\hat{f}_0 = 0.5$ only when $M = 0$). When the amplitude is large, the large separation resulting from the nominal parameters according to the numerical solutions violates the assumption of small-time fraction of a period where the pulley and shaft are disengaged.

4.1. First primary resonance

By considering the first primary resonance $\Omega = \Omega_1 + \varepsilon\sigma$ and following the aforementioned perturbation procedures and assumptions, one can obtain an analytical approximation for the first primary resonance. On the frequency–response curve, the maximum amplitude of approximation is the same as the linear solution, but the peak bends slightly to the left and all solutions are stable. In contrast, the numerical results in Ref. [1] form a complicated bifurcation diagram with alternate stable and unstable branches and the amplitude is distinguished markedly from the linear one. There are several reasons that the first primary resonance approximations are poor. First, the small separation assumption is not appropriate based on numerical results. Second, around the first primary resonance, not only the first mode but the second mode is excited. According to the frequency spectrum in Ref. [1], the highest spike occurs at the excitation frequency $\Omega \approx \Omega_1$ and comparably high spikes occur around Ω_2 as well. Through the perturbation procedures, the first primary resonance does not show second-mode participation ($a_2 \to 0$ as $t \to \infty$). Third, the harmonic resonance assumption cannot capture multiple disengagements or higher harmonic components. The numerical results indicate that near the first primary resonance, for a given excitation frequency Ω, the response not only includes the fundamental frequency Ω but frequency components at 4Ω, 5Ω or 6Ω with high amplitudes, where the multiple of Ω depends on the lobe location [1].

4.2. Impact of preload on the system dynamics

Preload M is an important design parameter. Positive preload is a practical requirement that guarantees the desired power transmission from the pulley to the accessory. The higher the preload is, the less disengagement occurs during a cycle.

We investigate the impact of the preload on the second primary resonance. If all the Fourier coefficients are zero, i.e., $f(\delta\theta) = 0$, the system response is linear. Given the linear amplitude according to Eq. (33), $a_2 = 4.3 \times 10^{-5}$, the Fourier coefficient curves from Eq. (19) with varying preload are obtained, which shows that $M \geqslant 0.0377$ prevents disengagement. The critical preload can be analytically determined by setting $\hat{f}_k = 0$ in Eq. (19), which causes $\cos\kappa_1 = 1$, and from Eq. (18):

$$M_{\mathrm{cr}} = -\frac{\gamma_2 a_2}{(\gamma_1^2/\Omega_1^2 + \gamma_2^2/\Omega_2^2)}. \tag{34}$$

Eqs. (33) and (34) imply that, for the given system, any set of excitation amplitude and damping ratio admits a critical preload beyond which the system behaves linearly at the second primary resonance. If $M \leqslant 0$, the numerical methods cannot yield steady state periodic solutions, while the perturbation procedure is not applicable because disengagement would be the leading motion between the pulley and shaft and this violates the basic assumptions.

Fig. 5 illustrates that large positive preload weakens the softening nonlinearity, and the perturbation method predicts good approximations. In contrast, low preload, for example, $M = 0.0127$ in Fig. 3, causes strong softening nonlinearity and the perturbation approximations are poorer. For $M \geqslant 0.0377$, the response overlaps the linear solution curve. Fig. 6 compares the time histories and the associated spectra of the relative displacements at points P_6 (in Fig. 3) and P_8 (in Fig. 5) from harmonic balance. The fraction of the period where the pulley and shaft are disengaged is not small for P_6 ($M = 0.0127$). In addition, the second harmonic of the response in Fig. 6(d) is not small, which implies the assumption of harmonic is not practical. On the other hand, the time history and spectrum of the response when $M = 0.0277$ at P_8 validates those assumptions, and perturbation is effective.

4.3. Impact of damping on the system dynamics

According to Eq. (22), the damping ratio does not influence the backbone curve. From Eq. (33), however, it does impact the response amplitude. When increasing the damping ratio ς (or μ), the two branches from Eq. (22) or from Eq. (31) close at a lower amplitude a_2. For low amplitude, the backbones of the numerical results and the approximations deviate only slightly, and the disengagement fraction of a period from harmonic balance is comparably small. In this case, perturbation generates good approximations. Fig. 7 verifies this claim by setting $\varsigma = 5\%$.

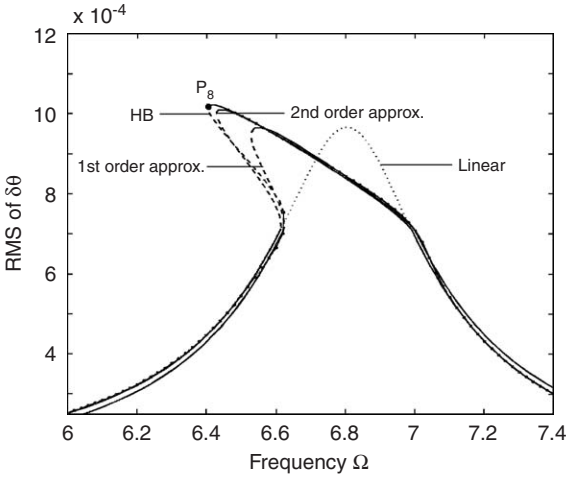

Fig. 5. The rms of $\delta\theta$ at the 2nd primary resonance, yielded by the method of multiple scales and harmonic balance for $M = 0.0277$ and other parameters in Table 1. Stable (——); unstable (- - -).

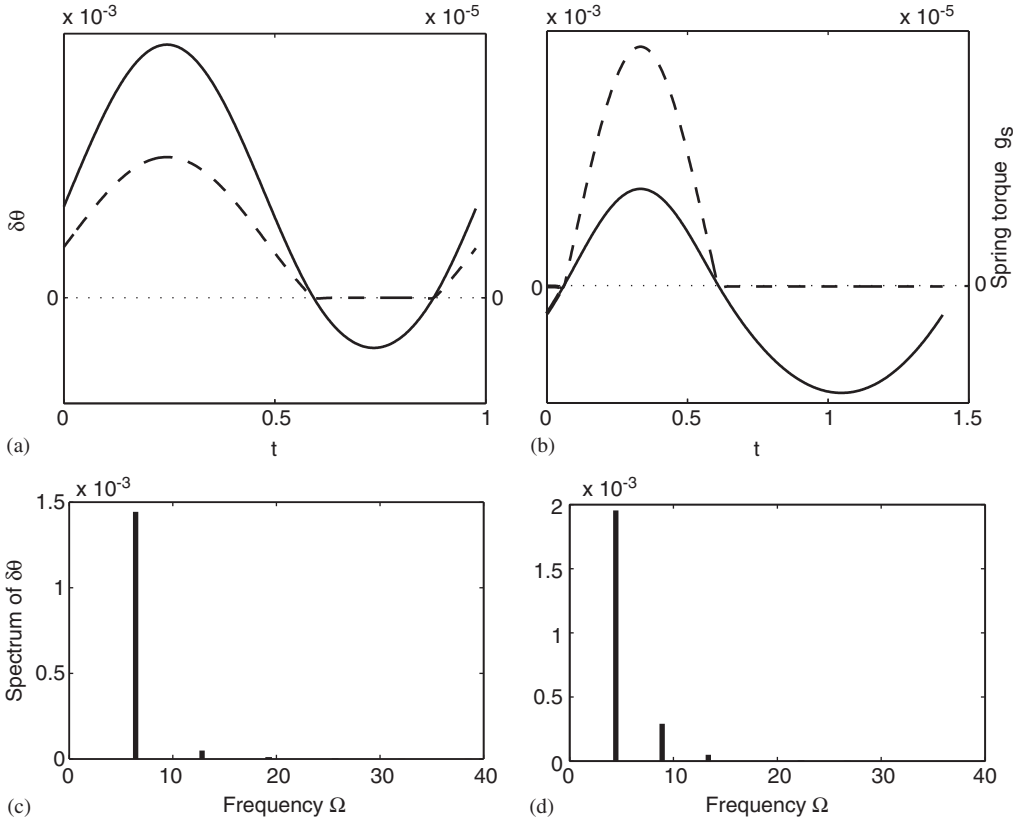

Fig. 6. Time history of $\delta\theta$ (—), spring torque $g_s(\delta\theta)$ (- -) and spectrum of $\delta\theta$. (a) and (c) for point P_8 as $\Omega = 6.42$ in Fig. 5 with $M = 0.0277$; (b) and (d) for point P_6 as $\Omega = 4.455$ in Fig. 3 with $M = 0.0127$.

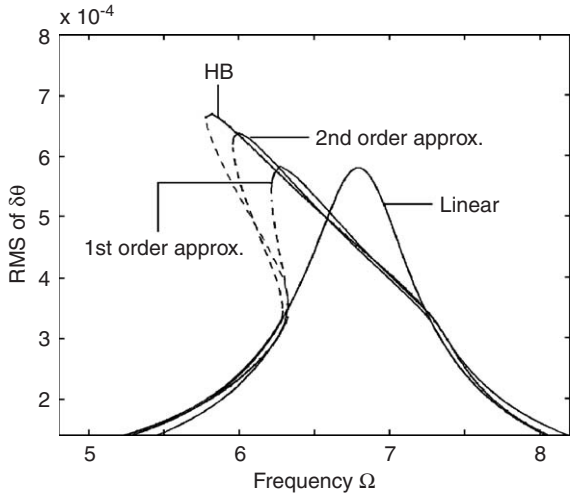

Fig. 7. The rms of $\delta\theta$ at the 2nd primary resonance, yielded by the method of multiple scales and harmonic balance for $\varsigma = 5\%$ and other parameters in Table 1. Stable (—); unstable (- -).

5. Summary and conclusions

A classical perturbation technique, the method of multiple scales, is employed to approximate the steady-state periodic solutions of a two-pulley belt system with clearance-type nonlinearity. The discontinuous separation function is expanded as a Fourier series in the perturbation analysis. For given amplitude, the Fourier coefficients of the separation function can be evaluated, and the closed-form frequency–response relation is determined at the first order. For the second-order approximation, the frequency–response relation is an implicit expression of a fourth-order polynomial.

The preload determines the softening level of the nonlinearity. Larger preload induces less disengagement, hence, less softening. In this case, the perturbation method generates good approximations. In contrast, lower preload results in a large disengagement fraction of a cycle, and therefore, greater softening deformation of the resonant peak. This degrades the small disengagement assumption and the perturbation approximations, including the amplitude and the backbone, deviate from the numerical solutions.

Acknowledgment

The authors are grateful to Mark IV Automotive/Dayco Corporation for their support.

References

[1] F. Zhu, R.G. Parker, Nonlinear dynamics of a one-way clutch in belt-pulley systems, *Journal of Sound and Vibration* 279 (1) (2005) 285–308.
[2] M. Senator, C.N. Bapat, A perturbation technique that works even when the non-linearity is not small, *Journal of Sound and Vibration* 164 (1) (1993) 1–27.
[3] J.-H. He, A new perturbation technique which is also valid for large parameters, *Journal of Sound and Vibration* 229 (5) (2000) 1257–1263.
[4] H. Hu, A classical perturbation technique which is valid for large parameters, *Journal of Sound and Vibration* 269 (2004) 409–412.
[5] S.H. Chen, Y.K. Cheung, A modified Lindstedt–Poincare method for a strongly non-linear two degree-of-freedom system, *Journal of Sound and Vibration* 193 (4) (1996) 751–762.
[6] S. Natsiavas, S. Theodossiades, I. Goudas, Dynamic analysis of piecewise linear oscillators with time periodic coefficients, *International Journal of Non-Linear Mechanics* 35 (2000) 53–68.
[7] S. Theodossiades, S. Natsiavas, Non-linear dynamics of gear-pair systems with periodic stiffness and backlash, *Journal of Sound and Vibration* 229 (2) (2000) 287–310.
[8] J.C. Ji, C.H. Hansen, Analytical approximation of the primary resonance response of a periodically excited piecewise non-linear–linear oscillator, *Journal of Sound and Vibration* 278 (2004) 327–342.
[9] A.H. Nayfeh, D.T. Mook, *Nonlinear Oscillations*, Wiley, New York, 1995.
[10] A. Hassan, Use of transformations with the higher order method of multiple scales to determine the steady state periodic response of harmonically excited non-linear oscillators, Part I: transformation of derivative, *Journal of Sound and Vibration* 178 (1) (1994) 1–19.
[11] A. Hassan, Use of transformations with the higher order method of multiple scales to determine the steady state periodic response of harmonically excited non-linear oscillators, Part II: transformation of detuning, *Journal of Sound and Vibration* 178 (1) (1994) 21–40.
[12] A. Hassan, A second comparison of two higher order perturbation schemes, *Journal of Sound and Vibration* 184 (5) (1995) 907–928.
[13] A. Luonga, A. Paolone, On the reconstitution problem in the multiple time-scale method, *Nonlinear Dynamics* 19 (1999) 133–156.